doi:10.1038/nature11697

Karl G. Janksy Very Large Array (VLA)[31]:

Three VLA observations were taken (see Supplementary Table 3). In all cases, the array was in the relatively compact C-configuration, and we used 3C48 to calibrate both the amplitude scale and the instrumental bandpass, and J0038+4137 to calibrate the antenna amplitude and phase gains. The cycle time between calibration scans was 6 minutes, spending 290 s on target and 70 s on calibrator in each cycle. The target was offset by 7 arcseconds from the field center, to eliminate the possibility of artifacts, generated at the phase center by correlation errors, affecting our measurements.

The original, discovery observation was taken on February 26, 2012 (MJD: 55983) with extremely good weather conditions; clear skies, wind 2.4 - 4.1 km/s, and the API (the atmospheric phase interferometer) showing phase noise of only 0.9-1.9 degrees. This one-hour track was observed in two 1024-MHz basebands centred at 5.256 GHz (at a resolution of 3.7 × 2.5 arcsec) and 7.45 GHz (at a resolution of 4.95 × 3.49 arcsec), and yielded highly significant detections of 338 ± 14 μJy/beam and 371± 8 μJy/beam respectively (quoted uncertainties at the 1σ level). Images were made using Briggs weighting with a robust factor of 0.5. Two iterations of phase-only self-calibration were performed on short (1-minute) timescales, before longer-timescale amplitude and phase self-calibration was carried out to remove amplitude errors around the two bright, confusing sources in the field.

A second one-hour observation taken on March 4 (MJD: 55990) found the emission to have decayed significantly, giving a weaker detection of 57 ± 18 μJy/beam (error of 1σ) when stacking the two C-band basebands. In the 3, 21, 26, and 41 GHz bands, we found 3σ upper

limits of 0.17, 0.09, 0.10, and 0.30 mJy/beam respectively. Since the 5.256 and 7.45-GHz detections were only 0.06 mJy/beam, none of these upper limits are constraining. Stacking the data from the 21 and 26-GHz bands, the nominal flux at the source position is -11 μJy/beam with a 1σ noise level of 24 μJy/beam. This high-frequency non-detection suggests a steep rather than inverted spectrum although this is far from conclusive.

A subsequent 30-minute observation taken on March 17 (MJD: 56003) confirmed the radio rebrightening suggested by the AMI-LA monitoring, with observed flux densities of 198 ± 15 μJy/beam at 7.45 GHz, and a less significant detection of 108 ± 33 μJy/beam at 5.256 GHz . As seen in the first VLA observation, the resulting spectrum is inverted. Importantly the emission was bright enough to trigger the subsequent VLBA observation.

Short timescale variability was only seen in the first of the VLA observations (Figure 2), and we did not see any evidence for significant variability in either the VLBA data or in the final two VLA observations, suggesting that the variability is intrinsic to the source rather than an instrumental artifact. However, to confirm this tentative conclusion, we performed an extensive array of tests to ensure that the reported variability in the first observation was genuine.

1. *Check sources:* A key test to differentiate intrinsic source variability from instrumental or calibration artifacts would be to demonstrate that the observed short-timescale variations were not seen in any other sources in the field. While there are four other unresolved sources in the field that are detected in both the 5.256 and 7.45-GHz images, the rapid decrease of antenna response beyond 1.5 arcmin from the pointing centre means that only the central two sources (within 2 arcmin) can act as reliable check sources, as time-variable pointing errors

due to wind loading of the antennas can cause large amplitude variations at larger distances from the pointing centre.

To investigate the relative variability of our target and check sources, we considered the total range of flux densities measured in the light curves, and tested the statistical level at which a constant source is excluded by performing a χ^2 test (summing $\Sigma_i[(S_i-<S>)/\sigma_i]^2$ over all data points). At 7.45 GHz, the total range of flux densities measured for the ULX was a factor of 2.5 greater than that measured for any of the check sources. The χ^2 test showed that the only source for which we could convincingly rule out the null hypothesis of a constant light curve at a statistically significant level (> 95% confidence) was the ULX, providing strong evidence that the variability seen at 7.45 GHz is real. For the 7.45 GHz data, the χ^2 value (for 22 degrees of freedom) was 108.2, implying that the null hypothesis (a constant source) is excluded at greater than 1 part in 10^{19}. For the 5-GHz data, the χ^2 value was 38.3, implying that probability of the null hypothesis (a constant source) being correct was 3 parts in 10^6. Thus we are confident that the observed short-timescale variability is real.

2. *Calibration errors*: When binning the data into 6-minute intervals, the amplitude and phase gain solutions on the phase calibrator source were extremely constant in time, so we cannot attribute the observed short-timescale variability to rapidly-changing gain solutions derived using the phase calibrator. Indeed, when blanking every other observation of the phase calibrator, the light curves derived for the target source did not change significantly. Furthermore, the light curves measured for the two independent circular polarisations were identical to within the statistical uncertainties. Additionally, the noise level in the images was constant in time to within 5 μJy/beam, except for the last, shorter time interval, where it rose significantly owing to the reduced exposure time, demonstrating that the short-timescale

variability was not caused by overall amplitude fluctuations in the image. Finally, we also checked the effect of carrying out the long-timescale amplitude and phase self-calibration. Since our target source flux density was less than 2% of the total flux density in the image at both frequencies, the self-calibration solutions would be expected to be dominated by the other, constant, sources in the field. A comparison of the light curves of the target source made with and without self-calibration indeed showed that it had no significant impact on the observed variability.

3. RFI: As a final test, we investigated the effect of radio frequency interference (RFI) on our light curves. RFI is a narrow-band, time-variable contaminant to the measured visibilities, and could in principle cause spurious variability. While the data were carefully edited to remove any signatures of RFI prior to the external gain calibration, there remains the possibility that spillover of bright RFI from flagged frequency channels into neighbouring channels could have left low-level contamination in the data. To rule out this scenario, we re-ran our analysis omitting any 128-MHz sub-bands that showed any signature of RFI. This left only three of eight sub-bands in the 5.256-GHz baseband, and only two of eight in the 7.45-GHz baseband. While the image noise was higher owing to the reduced bandwidth, the light curves were consistent within uncertainties with those made at full bandwidth, suggesting that RFI was not causing spurious variability.

Very Long Baseline Array (VLBA)[34]:

Following the confirmation of the radio rebrightening, we triggered an 8-hour VLBA observation on March 22 2012 (MJD: 56008), using the new wideband backend system to provide a total bandwidth of 256 MHz centred at 8416 MHz in each of two independent circular polarizations, using 2-bit sampling. We used J0038+4137 as a phase reference

calibrator (0.83 degrees from the ULX), but further refined the antenna gain solutions by using 5C 3.111 (2 arcminutes from the ULX) as an in-beam calibrator. The self-calibration model included only 5C 3.111. The data were correlated with two separate phase centres, one for the ULX, and one for 5C 3.111. With the available frequency resolution (0.5 MHz channels) and time resolution (2 s), time and bandwidth smearing would have diminished the signal of the ULX in the 5C 3.111 data set to the point where it would not have been detected. Therefore we did not include the ULX in the self-calibration model for 5C 3.111.

Phase solutions on 5C 3.111 were first derived on a 5-minute timescale, and were applied, following which we derived amplitude-and-phase solutions on a 20-minute timescale. Applying these calibration solutions to the ULX made only a 10% difference in the measured flux density of the ULX (increasing it from 0.20 ± 0.02 mJy/beam to 0.22 ± 0.02 mJy/beam). To aid the reader, we provide a VLBA contour plot of 5C 3.111 in Supplementary Figure 1. The contours are at levels of $\pm (\sqrt{2})^n$ times the lowest contour level of 25 μJy/beam, where n=3,4,5,... The peak flux density in the image is 11.3 mJy/beam. The selfcal solutions are dominated by the bright central point source (the extension to the south has a maximum brightness of only 0.2 mJy/beam, less than 2% of the peak).

The ULX was detected as an unresolved source at the 11σ level, with a measured brightness of 0.218 ± 0.021 mJy/beam with a beam size of 2.002×1.163 mas. This implies a brightness temperature limit of $> 3\times10^6$ K. There was no significant evidence for variability in the VLBA data. The astrometric position for the ULX was derived relative to J0038+4137 (assumed position RA=00h38m24.843587s, Dec = 41d37'06.00021"), and prior to running any self-calibration on 5C 3.111 (i.e. prior to applying the amplitude and phase gains derived using 5C 3.111, since self-calibration can in principle shift positions by a small fraction of a

beam). The ULX position was found to be within the *Chandra* X-ray error circle[35] at: RA = 00h42m43.674360(6)s, Dec = 41d25'18.70373(8)". The astrometric errors here are purely statistical, and quoted at the 1σ level. For the calibrator-target throw of 0.83 degrees, we estimate the systematic errors[36] to be < 45 microarcseconds. Adding the systematic and statistical errors linearly gives a final position of: RA = 00h42m43.674360(9)s, Dec = 41d25'18.7037(1)".

An elliptical Gaussian fit to the ULX in the image plane using the AIPS task JMFIT gives a size constraint of $< 1.3 \times 0.6 \text{mas}^2$, with a nominal major axis of 0.8 mas along position angle 138 degrees, and an unresolved minor axis. Fitting in the *uv*-plane using modelfit in Difmap gives a major axis of size 0.9-1.1 mas along position angle -44 to -49 degrees, with the minor axis again unresolved. While both fits suggest a resolved major axis, an unresolved source could not be ruled out, given the uncertainties on the best fitting parameters.

Arcminute Microkelvin Imager - Large Array (AMI-LA)[37]:

The AMI-LA has a nominal bandwidth centred at 15 GHz and divided into six usable equal-bandwidth channels of 0.75 GHz spanning 13.5 to 18 GHz. A two hour track by AMI-LA was taken the day following the first observation (February 27, MJD: 55984), yielding a detection of 500 ± 30 μJy/beam at 15 GHz (error of 1σ). Several weeks of monitoring followed this detection, finding a re-brightening to have occurred on March 10 (MJD: 55996), as confirmed by the final VLA detection. Since the resolution of AMI-LA is only 45 arcseconds, the proximity and brightness of 5C 3.111 restricted the achievable dynamic range in the region around the ULX. The ULX flux densities were therefore derived by comparing the pixel value at the VLBA position of the ULX with the rms noise measured in that region of the image.

Combined Array for Research in Millimeter-wave Astronomy (CARMA)[38]:

Observations of BHXRB jets have shown the synchrotron emission to extend in an unbroken power-law from the near-infrared down to energies at which self absorption dominates[39]. As CARMA operates at high radio frequencies, this provides an opportunity to constrain the broad-band synchrotron emission from such outflows. The CARMA correlator contains 8 bands, each configured to have 487 MHz bandwidth for optimal continuum sensitivity. The substantial drop in activity detected by AMI-LA in early March was confirmed in the CARMA 3 mm band (centred at 92 GHz), with no detection down to a 3σ upper limit of 0.33 mJy/beam on March 3-4 (MJD: 55989-55990). Subsequent observations on March 27 and 29 (also at 92 GHz, MJD: 56013 and 56015) also showed no detection, to a 3σ upper limit of 0.48 mJy/beam.

X-ray observations:

Several observations of the source were taken by *XMM-Newton*[40] (6), *Chandra* ACIS (1)[35] and *Swift*[41] XRT (14), with the observational parameters being described in Supplementary Table 1. We note that, although the full duration of the outburst is unknown, the observed X-ray light curve (Figure 1) appears broadly consistent with those seen during outbursts of Galactic LMXBs[42].

We fit the *XMM-Newton* and *Swift* data using the spectral analysis package, Xspec[43], testing standard BHXRB models for single power-law emission (*po* in Xspec), disc emission (*diskbb* in Xspec), disc emission plus power-law (*diskbb+po*) and disc emission plus thermal Comptonisation (*diskbb+compTT*). In each case we include a neutral absorption column (*tbabs* in Xspec) with the lower limit set to the Galactic line-of-sight column[44] and the best

available abundance tables[45]. We find that the first *XMM-Newton* observation when the source was detected (XMM 2) can be fully described by a hard power-law, whereas the outburst observations (XMM 3-4) are best described by emission from a disc with the seed photons Comptonised in a relatively cool population of thermal electrons. The latter is a highly significant improvement over describing the spectral data with *diskbb+po* ($\Delta\chi^2$ of 8 and 59 for each observation, respectively, for an increase of 1 degree of freedom) and is similar to fits obtained for other low-luminosity ULXs and high mass accretion rate BHXRBS[3,13,15,46]. Following the outburst, the *Swift* and *XMM-Newton* data are best described by a single disc component with a temperature very similar to that of high mass accretion rate BHXRBs[9]. We note that we do not detect the presence of any strong edge or line features in any of the X-ray spectra. In addition, we cannot constrain the presence of significant variability in any of the X-ray lightcurves, consistent with observations of other ULXs at similar luminosities[15].

The unabsorbed luminosities from these models (found by including the Xspec component, *cflux*) are given in Supplementary Table 1, and interesting parameters for the best-fitting model in each case (and how each observation corresponds to Figure 1) are given in Supplementary Table 2. For XRT observations 6-14, the data were not of a high enough quality to allow for individual fits and so we fit these simultaneously with XRT 1-5 allowing only the temperature to vary. As a result these luminosities should be treated with caution. However, as the luminosity obtained from an *XMM-Newton* observation (XMM 5) is very close to that obtained by XRT (13) at a very similar epoch, this implies that the quoted luminosities are in fact reasonable estimates.

Following the outburst (XMM 3-4), the X-ray spectrum and luminosity remained remarkably stable on long timescales across five *Swift* observations (XRT 1-5), unlike the lower-frequency radio emission. Of particular importance is the *Swift* observation (XRT 4) that is contemporaneous with the VLA and CARMA non-detections. In addition, a *Chandra* HRC-I observation taken 3 days after the radio rebrightening on March 10, demonstrated that the source had remained bright (with a crude estimated unabsorbed luminosity of $\sim 8\times10^{38}$ erg s^{-1}) in the X-rays (due to the lack of spectral data we do not include this in Figure 1).

By inspecting the behaviour of disc temperature against the unabsorbed luminosity we can see that the emission does not adhere to the $L \propto T^4$ relation seen in BHXRBs at sub-Eddington rates[9] but appears to invert or flatten at the highest luminosities (in XMM(3-4); see Supplementary Figure 2). This trend has been seen in the X-ray spectra of both ULXs[47,48] and in the very high state of some stellar-mass black hole X-ray binaries[49], thus supporting our identification of the source.

Short-timescale radio variability:

1) Brightness Temperature:

Having established the short-timescale variability as being intrinsic to the source, we can use it to determine the variability brightness temperature and hence constrain the relativistic beaming factor.

Since the brightness temperature is defined as $T_b = S_\nu c^2/(2k_B \nu^2 \Omega)$, we can determine the source size from the variability timescale (the light crossing time), and parameterize the brightness temperature as $T_b = 1\times10^{14}\ (\Delta S/\mathrm{mJy})\ (d/\mathrm{kpc})^2\ (\Delta t/\mathrm{s})^{-2}\ (\nu/\mathrm{GHz})^{-2}$ K, where ΔS is the flux density change at frequency ν in time Δt, and d is the source distance. For our source,

Figure 2 shows a flux density change of 0.21 mJy in 30 minutes at 7.45 GHz, giving a brightness temperature of $T_b = 7\times10^{10}$ K.

While typical Galactic BH XRBs have brightness temperatures determined from resolved VLBI imaging of $T_b < 1\times10^9$ K, there are examples of higher brightness temperatures derived from variability considerations. The well-established 30-minute oscillations in GRS 1915+105[25] (to which we have compared our observations) have brightness temperatures of $T_b = 5\times10^9$ K. However, the BHXRB, V4641 Sgr, has been detected to have a flux density variation of $\Delta S = 24$ mJy at 8.4 GHz in only 4 min[32]. At a source distance of 10 kpc[27], this equates to $T_b = 6\times10^{10}$ K, the same level as we have detected in our ULX. Thus our derived brightness temperature is not unprecedented for a stellar-mass BHXRB.

2) Detection probability: Variability brightness temperatures[33] scale as δ^3 (where $\delta=[\gamma(1-\beta\cos i)]^{-1}$ is the Doppler factor). The observed variability brightness temperature for our ULX is 7×10^{10} K, whereas the "standard" brightness temperature for BHXRBs is 1×10^9 K, implying a beaming factor of $\delta^3=70$. For an assumed jet speed, we can solve for the required inclination angle to observe the required beaming. For representative jet speeds in the range 0.90-0.98c, the inferred inclination angles are in the range 6-14 degrees. The probability of observing such an event (assuming a uniform distribution of angles to the line of sight) is in the range 0.5-3%. If instead we take the variability brightness temperature of GRS 1915+105 (5×10^9 K) as the reference unbeamed value, the acceptable inclination angles rise to 21-24 degrees, for a probability of 6-8%.

Alternatively, the peak brightness we observed at 780 kpc was 0.4 mJy (corresponding to a few Jy at 10 kpc; a level at which only 5-10 XRBs in our own Galaxy have been detected

over the past 20 years). In that time, we have detected outbursts from of order 50 BH and BH candidate XRBs in our own Galaxy, so for a similar population, the probability of detecting such an event is ~10-20%. Since the two estimates are in rough agreement, we estimate a likelihood of detecting the event we observed as a few percent.

Assuming that the VLA can detect such events down to an rms noise level of 5 μJy/beam (feasible in an hour's observing time, assuming 50% overheads), the 3σ detection threshold is then 15 μJy/beam, a factor of 26 below our peak flux. Thus we could detect such an event out to 5 times the distance of M31, i.e. ~4 Mpc. Thus, given the calculated probabilities, we can expect other detections in nearby galaxies, given suitable X-ray/radio monitoring campaigns to detect these sorts of outbursts.

3) The short-timescale variability and the size of the emitting region

The observed variability on timescales of several minutes could either be due to intrinsic variations (a variation in the jet speed, electron density, magnetic field, or orientation), or to interstellar scintillation as the signal passes through the turbulent, ionised interstellar medium of our Galaxy[50]. In the case of intrinsic variations, light-crossing time arguments would imply a source size of order 40 light minutes, corresponding to 5 AU, or a few microarcseconds at the distance of M31.

Should the observed variations be intrinsic, and due to a bending of the jet modifying its orientation to the line of sight and hence the Doppler boosting, we can calculate the angle change required. For a jet speed in the range 0.92-0.98c, we require a change in inclination angle of only 3-8 degrees. While this is a plausible scenario to explain the intrinsic variability, the current data do not allow us to determine whether this is the correct

explanation. Regardless, the source size constraint from the light-crossing time argument still holds as long as the variability is intrinsic.

Although scintillation is not typically seen in Galactic XRBs, the increased distance to M31 implies an angular size 100 times smaller, such that scintillation might be observed from any relatively compact jet emission. To ascertain whether the observed variability was consistent with what would be expected from scintillation, we used the large bandwidth of the VLA to compute the dynamic spectrum of the source in each of the two basebands, and performed two-dimensional correlation analyses on the dynamic spectra in time-frequency space[51]. The normalised covariance function should show extended features, whose widths in time and frequency give the variability timescale and decorrelation bandwidth of the signal respectively. Should these scale as expected from Kolmogorov turbulence, it would be good evidence that scintillation was responsible for the observed variability. From the variability timescale, we could then derive an upper limit on the source size. While we detected the variability timescale at both frequencies, the decorrelation bandwidth was unconstrained at 7.45 GHz. Thus, while our results were consistent with the expectations of scintillation, there were again too few independent variations in the data to definitively determine the mechanism responsible for the observed short-timescale variability. However, if scintillation was the cause, then for typical scattering screen parameters (a distance d_s of 100 pc and a velocity v_s of 50 km s^{-1}), the measured variability timescale ($t=\theta\, d_s/v_s$) implies a source size θ of 3 microarcseconds.

Thus, regardless of the origin of the short-timescale variability (intrinsic or scintillation), we can place a limit of a few microarcseconds (a few AU at the distance of M31) on the size of the emitting region.

Supplementary References

[31] http://www.aoc.nrao.edu/evla/

[32] Rupen, M.; Mioduszewski, A. & Dhawan, V. Strong radio flare in V4641 Sgr (= SAX J1819.3-2525). **ATel #172**, http://www.astronomerstelegram.org/?read=172 (2003)

[33] Readhead, A. Equipartition brightness temperature and the inverse Compton catastrophe. *Astrophys. J.*, **426**, 51-59 (1994)

[34] http://www.vlba.nrao.edu/

[35] Barnard. R; Garcia M. & Murray S. A Chandra/ACIS observation of the transient M31 ULX XMMU J004243.6+412519. **ATel #3937**, http://www.astronomerstelegram.org/?read=3937 (2012)

[36] Pradel, N.; Charlot, P. & Lestrade, J.-F. Astrometric accuracy of phase-referenced observations with the VLBA and EVN. *Astron. Astrophys*, **452**, 1099-1106 (2006)

[37] http://www.mrao.cam.ac.uk/telescopes/ami/

[38] http://www.mmarray.org/

[39] Falcke, H.; Körding, E. & Markoff, S. A scheme to unify low-power accreting black holes. Jet-dominated accretion flows and the radio/X-ray correlation. *Astron. Astrophys.*, **414**, 895-903 (2004)

[40] http://heasarc.gsfc.nasa.gov/docs/xmm/xmmgof.html

[41] http://swift.gsfc.nasa.gov/docs/swift/swiftsc.html

[42] Done, C.; Gierliński, M. & Kubota, A. Modelling the behaviour of accretion flows in X-ray binaries. Everything you always wanted to know about accretion but were afraid to ask. *Astron. Astrophys. Rev.*, **15**, 1-66 (2007)

[43] Arnaud, K.A. Astronomical Data Analysis Software and Systems V, eds. Jacoby G. and Barnes J., **101,** 17 (1996)

[44] Dickey, John M. & Lockman, Felix J. H I in the Galaxy Authors. *Ann. Rev. Astron. Astrophys.,* **28**, 215-261 (1990)

[45] Wilms, J.; Allen, A. & McCray, R. On the Absorption of X-Rays in the Interstellar Medium. *Astrophys. J.*, **542**, 914-924 (2000)

[46] Winter, L.; Mushotzky, R. & Reynolds, C. XMM-Newton Archival Study of the Ultraluminous X-Ray Population in Nearby Galaxies. *Astrophys. J.*, **649**, 730-752 (2006)

[47] Soria, R. Bridging the gap between stellar-mass black holes and ultraluminous X-ray sources. *Astrophys. S. Sci*., **311**, 213-222 (2007)

[48] Kajava, J. & Poutanen J. Spectral variability of ultraluminous X-ray sources. *Mon. Not. R. Astron. Soc*., **398**, 1450-1460 (2009)

[49] Kubota, A. & Done, C. The very high state accretion disc structure from the Galactic black hole transient XTE J1550-564, *Mon. Not. R. Astron. Soc.*, **353**, 980-990 (2004)

[50] Rickett, B. Radio propagation through the turbulent interstellar plasma. *IN: Ann. Rev. Astron. Astrophys.,* **28**, 561-605 (1990)

[51] Cordes, J. M. Space velocities of radio pulsars from interstellar scintillations. *Astrophys. J.*, **311**, 183-196 (1986)

Supplementary Table 1. Summary of the X-ray observations

Instrument (observation)	Observation ID	Date (MJD)	Unabsorbed (0.3-10keV) luminosity ($\times 10^{38}$ erg s^{-1})
XMM (1)	0674210301	2012-01-07 (55933)	< 0.2
XMM (2)	0674210401	2012-01-15 (55941)	2.0 ± 0.2
XMM (3)	0674210501	2012-01-21 (55947)	9.8 ± 0.2
XMM (4)	0674210601	2012-01-31 (55957)	12.6 ± 0.2
XMM(5)	0700380501	2012-07-28 (56136)	1.3 ± 0.1
XMM(6)	0700380601	2012-08-08 (56147)	0.7 ± 0.1
ACIS (1)	13837	2012-02-19 (55976)	10.8 ± 0.4
XRT (1)	00032286002	2012-02-19 (55976)	9.1 ± 0.5
XRT (2)	00032286003	2012-02-23 (55980)	9.7 ± 0.6
XRT (3)	00032286006	2012-03-02 (55988)	9.6 ± 0.4
XRT (4)	00032286007	2012-03-03 (55989)	9.1 ± 0.4
XRT (5)	00032286010	2012-03-04 (55990)	9.5 ± 0.5
XRT(6)	00035336052	2012-05-24 (56071)	4.4 ± 0.2
XRT(7)	00035336053	2012-06-01 (56079)	3.3 ± 0.2
XRT(8)	00035336054	2012-06-09 (56087)	3.5 ± 0.3
XRT(9)	00035336055	2012-06-17 (56095)	3.4 ± 0.3
XRT(10)	00035336056	2012-06-25 (56103)	3.5 ± 0.4
XRT(11)	00035336060	2012-07-15 (56123)	2.4 ± 0.4
XRT(12)	00035336061	2012-07-19 (56127)	2.3 ± 0.4
XRT(13)	00035336062	2012-07-27 (56135)	1.4 ± 0.2
XRT(14)	00035336063	2012-08-05 (56144)	1.1 ± 0.8

Dates and model unabsorbed luminosities for each X-ray observation of XMMU J004243.6+412519. In addition to the above, a further Chandra HRC-I observation was taken on March 13 which showed that the source was still X-ray bright (at $L \sim 8\times10^{38}$ erg s^{-1}) when the radio re-brightening occurred (although due to the lack of spectral resolution in this instrument we do not include it in Figure 1).

Supplementary Table 2. Best-fitting model parameters to the X-ray spectra

Instrument (obs) Corresponding panel in Figure 1	Best-fitting model				Fit quality: χ^2/dof (null hypothesis probability)
XMM(2) Panel *(b)*	tbabs*po				161.8/163 (0.51)
	nH ($\times10^{22}$ cm^{-2})	Index (Γ)			
	0.38 ± 0.07	2.0 ± 0.2			
XMM(3)	tbabs*(diskbb+compTT)				429.5/457 (0.82)
	nH ($\times10^{22}$ cm^{-2})	kT$_{disc}$ (keV)	kT$_{compt}$ (keV)	Optical depth (τ)	
	0.45 ± 0.02	$0.53^{+0.16}_{-0.28}$ L = 7.3×10^{38}erg s^{-1}	$1.21^{+0.25}_{-0.18}$	$11.9^{+2.1}_{-1.9}$	
XMM(4) Panel *(c)*	tbabs*(diskbb+compTT)				436.9/423 (0.31)
	nH ($\times10^{22}$ cm^{-2})	kT$_{disc}$ (keV)	kT$_{compt}$ (keV)	Optical depth (τ)	
	$0.44^{+0.02}_{-0.05}$	$0.59^{+0.18}_{-0.34}$ L = 10.2×10^{38}erg s^{-1}	$1.27^{+0.45}_{-0.33}$	$11.0^{+3.0}_{-2.6}$	
XRT(1-5) Panel *(d)*	tbabs*diskbb				205.1/203 (0.45)
	nH ($\times10^{22}$ cm^{-2})	kT$_{disk}$ (keV)			
	0.38 ± 0.03	0.89 ± 0.02			
XMM(5) Panel *(e)*	tbabs*diskbb				102.4/119 (0.86)
	nH ($\times10^{22}$ cm^{-2})	kT$_{disc}$ (keV)			
	$040^{+0.03}_{-0.04}$	0.45 ± 0.02			
XMM(6) Panel *(f)*	tbabs*diskbb				87.8/112 (0.96)
	nH ($\times10^{22}$ cm^{-2})	kT$_{disc}$ (keV)			
	0.39 ± 0.04	0.36 ± 0.02			

Parameters for each of the best fitting models to the high quality X-ray datasets (uncertainties quoted at the 90% level). In the case of XRT(1-5) we co-add the individual datasets to obtain a well constrained fit. We do not include fits to XRT(6-14) as the data quality is too poor to be fitted in a reliable manner.

Supplementary Table 3. Summary of VLA observations

Date	VLA band (GHz)	Flux density (μJy/beam)
2012-02-26	5.256	338 ± 14
	7.450	371 ± 8
2012-03-04	3.000	< 168
	5.256 + 7.450	57 ± 18
	20.800	< 87
	25.900	< 99
	40.988	< 312
2012-03-17	5.256	108 ± 33
	7.450	198 ± 15

Dates, bands and fluxes (with 1σ errors) for the three VLA observations. The observing bandwidth was 1024 MHz except at 41 GHz, where it was 2048 MHz. Both the first and third observations indicate an inverted spectrum whilst the spectrum in the second observation is unconstrained (the quoted upper limits are all at the 3σ level).

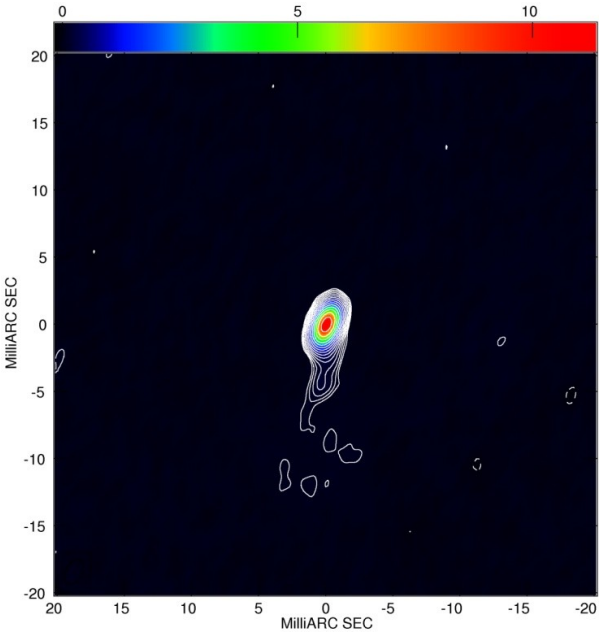

Supplementary Figure 1: VLBA image of 5C 3.111. We include this figure to help the reader understand the reliability of the ULX image presented in Figure 2. The contours are at levels of $\pm(\sqrt{2})^n$ times the lowest contour level of 25 μJy/beam, where n=3,4,5,... The peak flux density in the image is 11.3 mJy/beam. The self-calibration solutions are dominated by the bright central point source (the extension to the south has a maximum brightness of only 0.2 mJy/beam, less than 2% of the peak).

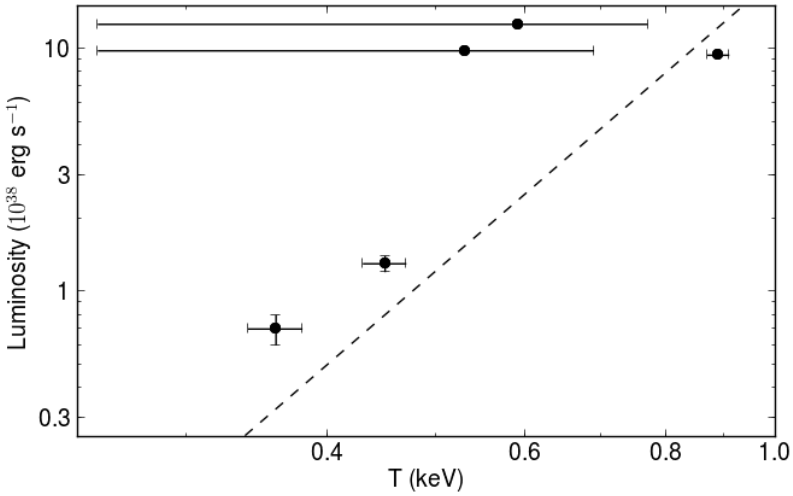

Supplementary Figure 2: Log space plot of unabsorbed luminosity versus peak disc temperature (values for which are given in Supplementary Tables 1 and 2) for XMM (3-6) and XRT (1-5). The increase in temperature between the highest luminosity spectrum and the disc dominated spectrum on the decay appears to match the behaviour seen in other low luminosity ULXs[47,48] and in the very high state of some stellar-mass black hole X-ray binaries[49], and is in contrast to that observed in sub-Eddington BHXRBs.